Three-dimensional simulation of laser-produced plasma for extreme ultraviolet lithography applications

V. Sizyuk,[a] A. Hassanein, and T. Sizyuk
Argonne National Laboratory, 9700 South Cass Avenue, Argonne, Illinois 60439

(Received 18 May 2006; accepted 21 August 2006; published online 30 November 2006)

Laser-produced plasma (LPP) from a tin target is being considered as the light source for the next generation of extreme ultraviolet (EUV) lithography. An integrated model was developed to simulate the plasma behavior and the EUV radiation output in LPP devices. The model includes plasma heat conduction and hydrodynamic processes in a two-temperature approximation, as well as detailed photon radiation transport using Monte Carlo methods. Multiple laser beams incident on a single target have been simulated in full three-dimensional geometry, using the total variation-diminishing scheme for the plasma hydrodynamics and an implicit scheme for heat conduction processes. Numerical simulations showed that EUV conversion efficiency increases for multiple-beam devices with specific optimum laser locations and direction compared to a single-beam device. © *2006 American Institute of Physics*. [DOI: 10.1063/1.2365717]

I. INTRODUCTION

Since the inventions of the transistor in 1947 and the integrated circuit in the late 1950s, the development of semiconductor technology has vastly accelerated. More transistors allow increased functionality, and smaller size allows increased switching speed and less power consumption for each transistor. One of the most important lithographic processes is exposure, when light shining on selective parts of the resist is used to draw microelectronic elements.[1] Resolution of an optical system such as a projection-lithography system is traditionally determined by the Rayleigh criterion, that is, with the wavelength of light and the numerical aperture of the optical system. Because increasing the numerical aperture has appreciable limitations, utilizing the smallest wavelength of projection lithography is key to progress in semiconductor technology. The current source wavelength for exposure in semiconductor manufacturing is 193 nm, produced by an ArF excimer laser. The next step requires developing and optimizing light sources at 13.5 nm in extreme ultraviolet (EUV) diapason.[2]

The EUV radiation can be generated by several methods: discharge-produced plasma (DPP), laser-produced plasma (LPP), and synchrotron radiation. Each method has advantages and disadvantages. In order to meet the requirements of the Intel lithography roadmap goals for high-volume manufacturing[3] and SEMATECH's EUV source program goal,[4] the EUV source is required to have power exceeding 180 W at a wavelength of 13.5 nm (2% bandwidth). Various LPP and gas DPP devices are under development and investigation.[5–9] At present, several of the EUV sources begin to realize the power level demanded by commercial chip manufacturers. The conversion efficiency (CE) of the EUV radiation is an important factor in the successful development of the source. Many additional factors are also important and influence the efficiency of the EUV device, such as the plasma material, form and size of the radiated area, collectable solid angle, and the amount of debris generated. Because many physical processes are involved and many technical problems need to be solved (laboratory experiments are very expensive) when optimizing a particular EUV device, only computer modeling can generate a complete insight to various design issues within a reasonable time. Moreover, integrated detailed physical models should be developed specifically for simulation of plasma behavior in discharge-produced and laser-produced EUV devices. The models should include and integrate several parts: atomic physics, hydrodynamics, radiation transport, heat conduction, and EUV analysis. An EUV source should be modeled completely, from the start of the input energy mechanism and plasma formation to the EUV output from the pinch or laser target and finally from the mirror collector system. Each physical process should be adequately described, with advanced and accurate numerical schemes that should be used for each physical process.

In this paper we present modeling results of LPP devices with up to three simultaneous incident beams. The model is based on previous progress in simulation of discharge- and laser-produced plasma devices of our high energy interaction with general heterogeneous target systems (HEIGHTS) package.[10–13] We have enhanced the HEIGHTS package so that the model can simulate any number of laser beams incident simultaneously on various target structures in full three-dimension geometry. Plasma hydrodynamics, radiation transport processes, heat conduction, and laser absorption processes are taken into account with fine details. The optimum location and direction of the laser beams are calculated for maximum EUV conversion efficiency. The CE of LPP devices is found to increase by using multiple lasers in comparison to the standard single-beam configuration with the same total laser energy.

[a]Author to whom correspondence should be addressed; electronic mail: sizyuk@anl.gov

 © 2006 American Institute of Physics

Downloaded 12 Dec 2006 to 140.221.12.207. Redistribution subject to AIP license or copyright, see http://jap.aip.org/jap/copyright.jsp

II. COMPUTATIONAL MODEL

The plasma motion dynamics were considered using the set of four conservation laws: mass density, momentum, energy, and magnetic field in the form of

$$\frac{\partial q}{\partial t} + \nabla \cdot \mathbf{F}_q = 0, \tag{1}$$

where q is the conservation parameter and $\mathbf{F}_q$ is the flux of this parameter. We use Gaussian units unless indicated otherwise. In application to plasma as a continuous, compressible medium, we expanded Eq. (1), and have the following expressions for conservation of mass, momentum, and total energy:

$$\frac{\partial \rho}{\partial t} + \nabla \cdot (\rho \mathbf{v}) = 0,$$

$$\frac{\partial}{\partial t}\rho \mathbf{v} + \nabla \cdot (\rho \mathbf{v}\mathbf{v} + p_h) = 0, \tag{2}$$

$$\frac{\partial e_h}{\partial t} + \nabla \cdot [\mathbf{v}(e_h + p_h)] = 0.$$

Here, ρ is the density of the plasma, $\mathbf{v}$ is the velocity of the plasma, p_h is the hydrodynamic pressure, and $e_h = \rho v^2/2 + e_{\mathrm{int}}$ is the sum of kinetic and internal energy densities of the plasma. Because we consider EUV lithography applications of the LPP with the radiation power density of $10^{10}-10^{11}$ W/cm^2 we ignored the influence of thermomagnetic processes on the plasma behavior.[12] After taking into account heat conduction and radiation transport, the general form of the hydrodynamic equation set is given in two-temperature approximation by

$$\begin{aligned}
&\frac{\partial \rho}{\partial t} + \nabla \cdot (\rho \mathbf{v}) = 0,\\
&\frac{\partial \rho \mathbf{v}}{\partial t} + \nabla \cdot (\rho \mathbf{v}\mathbf{v} + p_h) = 0,\\
&\frac{\partial e_h}{\partial t} + \nabla \cdot [\mathbf{v}(e_h + p_h) - \lambda_e \nabla T_e - \lambda_i \nabla T_i - \mathbf{S}_{\mathrm{rad}}] = Q_{\mathrm{las}},\\
&\frac{\partial e_i}{\partial t} + \nabla \cdot [\mathbf{v}(e_i + p_i) - \lambda_i \nabla T_i] = Q_{\mathrm{ei}},
\end{aligned} \tag{3}$$

Here, $e_h = e_e + e_i + e_{\mathrm{kin}}$ is the total energy, e_e is the electronic component of the plasma energy, which includes the thermal energy of electrons and ionization energy, e_i is the ion component of the plasma energy, and $e_{\mathrm{kin}} = \rho v^2/2$ is the kinetic energy of the plasma. Analogous to energy, pressure has electron and ion parts: $p_h = p_e + p_i$. We use the subscript e for electrons and i for ions. The thermal conduction in the plasma is considered as the combined result of the electron $\lambda_e \nabla T_e$ and ion $\lambda_i \nabla T_i$ components, where λ is the conductivity coefficient and T is the temperature. The radiation transport process is represented here as flux $\mathbf{S}_{\mathrm{rad}}$ and the laser heating source as Q_{las}. Also taken into account is the energy interchange between electrons and ions Q_{ei}.[14]

Equation (3) constitutes the initial set of equations used for modeling the laser-generated plasma processes. The conditions of a particular problem and specific geometry will lead to the transformation of these main equations. Because in this study we considered plasma devices and plasma motion that may not have symmetry, we expressed Eq. (3) in the three-dimensional Cartesian coordinate set system. Since the final set of the transformed equations has convective terms (hydrodynamic flux) and dissipative terms (heat conduction, laser heating, radiation transport, and electron-ion interaction), we used splitting methods in our numerical algorithm to separate the hyperbolic and parabolic parts.[12,13,15] As a result, the general solution algorithm has two stages: convective and dissipative. The transformed initial set of equations is given in matrix form as

$$\frac{\partial \mathbf{U}}{\partial t} + \frac{\partial \mathbf{F}(\mathbf{U})}{\partial x} + \frac{\partial \mathbf{G}(\mathbf{U})}{\partial y} + \frac{\partial \mathbf{H}(\mathbf{U})}{\partial z} = \mathbf{\Omega}, \tag{4}$$

where the solution field and hydrodynamic fluxes are

$$\mathbf{U} = \begin{bmatrix} \rho \\ \rho v_x \\ \rho v_y \\ \rho v_z \\ e_h \\ e_i \end{bmatrix}, \quad \mathbf{F} = \begin{bmatrix} \rho v_x \\ \rho v_x^2 + p_h \\ \rho v_x v_y \\ \rho v_x v_z \\ v_x(e_h + p_h) \\ v_x(e_i + p_i) \end{bmatrix},$$
$$\mathbf{G} = \begin{bmatrix} \rho v_y \\ \rho v_y v_x \\ \rho v_y^2 + p_h \\ \rho v_y v_z \\ v_y(e_h + p_h) \\ v_y(e_i + p_i) \end{bmatrix}, \quad \mathbf{H} = \begin{bmatrix} \rho v_z \\ \rho v_z v_x \\ \rho v_z v_y \\ \rho v_z^2 + p_h \\ v_z(e_h + p_h) \\ v_z(e_i + p_i) \end{bmatrix} \tag{5}$$

and the dissipative terms are combined in the source $\mathbf{\Omega}$,

$$\mathbf{\Omega} = \begin{bmatrix} 0 \\ 0 \\ 0 \\ 0 \\ Q_{i,\mathrm{th}} + Q_{e,\mathrm{th}} + Q_{\mathrm{rad}} \\ Q_{i,\mathrm{th}} + Q_{\mathrm{ei}} \end{bmatrix}. \tag{6}$$

Here $Q_{e,\mathrm{th}}$ is the electron heat conduction, $Q_{i,\mathrm{th}}$ is the ion heat conduction, Q_{rad} is the radiation transport, and Q_{ei} is the electron-ion interaction. The conservative form of the initial equations allows the use of the total variation-diminishing method in the Lax-Friedrich formulation (TVD-LF) (Refs. 16 and 17) for the solution of the convective stage given by Eq. (4). Following the splitting method, the Q terms in Eq. (6) are calculated separately with the second (dissipative) stage of the HEIGHTS solver and are used as correctors of the main TVD-LF solution. An implicit numerical scheme with sparse matrix linear solvers is used for calculating the terms $Q_{e,\mathrm{th}}$ and $Q_{i,\mathrm{th}}$.[12,13] The electron-ion interaction term $Q_{\mathrm{ei}} = 3(m_e n_e / m_i \tau_e)(k_B T_e - k_B T_i)$ is calculated for each hydrodynamic step and used as input in the right side of Eq. (6),

Downloaded 12 Dec 2006 to 140.221.12.207. Redistribution subject to AIP license or copyright, see http://jap.aip.org/jap/copyright.jsp

where m is the mass, n_e and τ_e are the electron concentration and the relaxation time, respectively, e is the electron charge, and k_B is the Boltzmann constant.

Monte Carlo methods are used for modeling the LPP radiation processes: the laser heating, the radiation transport in the plasma, and the EUV output. For LPP radiation transport, radiation fluxes must be determined to solve two main problems: (1) correction of the plasma thermal energy and, as a result, correction of the plasma motion in the device, and (2) determination of the final useful part of the radiation flux (EUV output). These problems determine the requirements for the flux data and the numerical techniques needed for solving the photon transport problem. Correct calculation of the energy spatial redistribution in full spectrum of the plasma plays a very important role in solving the first problem. The required model adequately describes radiation transport only if it takes into account the optical thickness of the plasma in a large number of spectral groups. The full spectrum of the LPP plasma is divided into narrow spectral groups with separate treatment of strong lines. The total number of the spectral groups was optimized to accurately describe the radiation energy redistribution for a reasonable computational power. As preliminary calculations show,[18] the results have an acceptable error for total spectral groups of $\sim 10^3$. However, such spectral groups are inapplicable for detailed investigations in the EUV band of interest, 2% at 13.5 nm. For this reason, we use two sets of optical opacities: general (for full-energy redistribution calculations) and specific (for calculations in a specific spectral band). The main hydrodynamic simulations use general opacity tables and calculate the evolution of the plasma temperature and density. The final EUV simulations use fine detailed opacities to calculate the LPP device efficiency.[19]

Studying the trajectory, as well as the number of emitted and absorbed energy portions at each point of the plasma domain (or the points of major interest), one may calculate the redistribution of energy due to photon transport. Because simulation of all photons in the domain is problematic (computation time and power are limited), each energy portion is assumed to be a monochromatic set of photons. Hence, a macrophoton has the properties (absorption and emission probabilities) of the component photons, and the energy is equal to the sum of all photon energies in the set. To optimize the algorithm and decrease computation costs, we introduced a system of weight factors into the Monte Carlo radiation transport model. Two major weight factors were allocated: normalization of the emitted macrophoton relative to most radiated cells of the computational domain and normalization relative to the optical thickness of a cell. The first weight factor is determined from the emission physics processes; it accelerates calculations because of the neglect of emission of cold cells. Because of the second weight factor, so-called idle processes are ignored, namely, situations involving the emission and the absorption of the photon in the same cell (absorbed lines). A third weight factor can be useful in the case of a strong nonuniform mesh. The volume of the emitting cell can be so small that the amount needed for simulating photon bundles will not be enough to obtain correct results. The volume weight coefficient should increase the computation accuracy in this case. More detailed description of the Monte Carlo radiation transport model is presented in Refs. 11 and 18.

As noted earlier, each macrophoton has properties similar to those of a real laser radiation photon. The action of each real photon cannot be simulated individually, however, because of the large number of real photons in the beam; hence, the action (energy transport) of a group of photons is combined into the macrophoton action. We estimate the number of real photons W_{macro} in a macrophoton from the required accuracy and the available computational power, that is, from the total number of available macrophotons N_{macro},

$$N_{\text{macro}} = \frac{N_{\text{real}}}{W_{\text{macro}}}, \quad N_{\text{real}} = \frac{P_{\text{las}}}{E_{\text{ph}}}. \tag{7}$$

Here P_{las} is the momentary laser power, and E_{ph} is the energy of one real laser radiation photon. The HEIGHTS integrated package takes into account both the time and space distributions of the laser pulse power. For square time distribution, the laser pulse power is given by

$$P_{\text{las}} = \frac{Q_{\text{pulse}}}{t_{\text{pulse}}}, \tag{8}$$

where the energy of the pulse Q_{pulse} is distributed uniformly over the pulse duration t_{pulse}. The Gaussian distribution in time is expressed as the function

$$P_{\text{las}}(t) = P_0 \exp\left[-\frac{(t-\sigma_t)^2}{\sigma_t^2}\right]. \tag{9}$$

It is assumed in this equation that the pulse duration is $t_{\text{pulse}}=2\sigma_t$. The maximum power P_0 can be calculated from the integral

$$P_0 = \frac{Q_{\text{pulse}}}{\int_0^\infty \exp[-(t-\sigma_t)^2/\sigma_t^2]dt}. \tag{10}$$

Assuming a round laser beam cross section, the spatial distribution of the laser radiation flux can be simulated as uniform and Gaussian along the radius. Most practical applications have Gaussian spatial distribution[20] of

$$I(r,t) = I_0(t)\exp\left(-\frac{r^2}{\sigma_s^2}\right), \tag{11}$$

where the pulse power distribution in time $P_{\text{las}}(t)$ is taken into account. Here it was also assumed that the radius of the beam is $r_{\text{beam}}=\sigma_s$.

The HEIGHTS package has a computation module to control the directional and focusing characteristics of multiple laser beams set incident on targets. Figure 1 schematically illustrates the three-dimensional computation domain with multiple laser beams directed onto a spherical target. To fully describe the spatial geometry of each laser beam, one needs to define the coordinates of the initial laser beam point $O_1(x_1,y_1,z_1)$, radius of the beam at the initial point r_1, final point $O_2(x_2,y_2,z_2)$, and final radius r_2. Moreover, the location of the focus point F of the laser beam must be defined, either inside or outside the $[O_1O_2]$ segment.

Because the HEIGHTS package considers laser absorption

Downloaded 12 Dec 2006 to 140.221.12.207. Redistribution subject to AIP license or copyright, see http://jap.aip.org/jap/copyright.jsp

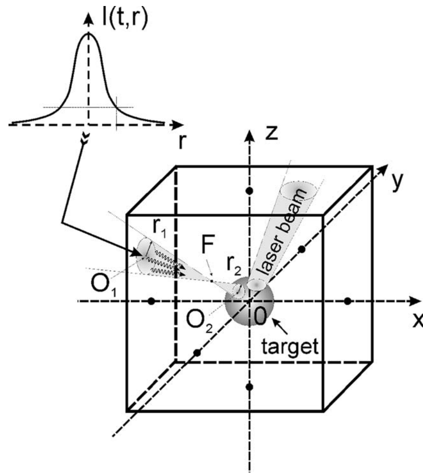

FIG. 1. Schematic illustration of three-dimensional modeling domain of LPP devices.

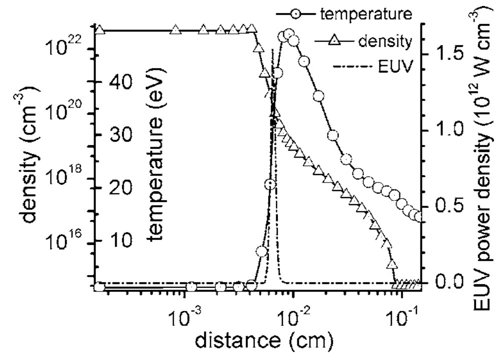

FIG. 2. Spatial distributions of the density, temperature, and EUV flux along the laser beam axis.

in a plasma cloud, the inverse bremsstrahlung was assumed as the main process by which the laser radiation was absorbed by plasma electrons. The classical value for the absorption coefficient $k_{\text{abs}}^{\text{las}}$ that describes the collisional absorption mechanism is[21]

$$k_{\text{abs}}^{\text{las}} = \frac{16\pi Z n_e^2 e^6 \ln \Lambda(\nu)}{3c\nu^2(2\pi m_e k_B T_e)^{3/2}(1-\nu_p^2/\nu^2)^{1/2}}, \tag{12}$$

where e, n_e, m_e, and T_e are the electron charge, density, mass, and temperature, respectively, Ze is the ionic charge, c is the light speed, ν is the frequency of the laser light, $\nu_p = \sqrt{n_e e^2/\pi m_e}$ is the plasma frequency, and k_B is the Boltzmann constant. The Coulomb logarithm is given by[22]

$$\ln \Lambda = \ln\left[\frac{3}{2}\sqrt{\frac{(k_B T_e)^3}{\pi n_e}}\frac{1}{Ze^3}\right]. \tag{13}$$

The condition $\nu_p \geqslant \nu$ at any spatial point is used during the simulation of photon reflection. The new direction of motion we sampled was isotropic.

To validate the model and to benchmark the enhanced HEIGHTS package, we solved several test problems and compared our results with analytical and experimental results. The calculation blocks (TVD-LF, thermal conductivity, radiation transport, etc.) were tested separately in various combinations.[10–13,18,23]

III. RESULTS AND DISCUSSIONS

For this study we focused our numerical modeling on a tin target material because of its current interest as the source for 13.5 nm EUV lithography.[24–26] Many investigators are trying to optimize the tin target geometry, laser pulse and prepulse characteristics, and device chamber design in order to increase the EUV output source efficiency, to mitigate the debris, and to improve the manufacturability of the total process. An ideal light source for the EUV lithography is a small spherical target with high enough density and with optimum temperature for maximum EUV output. This approach is used in many theoretical investigations to study the efficiency of the EUV emission and source improvement.[8,9] In reality, the EUV emission region is only a thin layer between areas with high temperature and low density and areas with high density and low temperature (Fig. 2). The size and form of the EUV region depend on many factors, such as target material, target structure, laser beam parameters, and spatial configuration of the LPP device. Enlarging and shaping of this region will enable researchers to increase the LPP device efficiency and to develop the required high EUV power source for lithography. Two ways are possible to expand the EUV area: (1) laser heating of the dense area to increase the temperature and (2) confinement of the rarefied area to increase the density. Laser heating of dense areas is being actively investigated.[27] Complex targets where the material combines clusters are proposed for laser heating and for decreasing the initial density of the target plasma. We present in this paper a theoretical examination of the second way to increase the final EUV efficiency of the LPP device.

A recent study observed an increase of EUV emission near a wall located close to the laser target.[28] In our opinion, this effect is attributable to the confinement of motion of the heated plasma: The density of the hot plasma increases near the wall, its temperature decreases without direct laser heating, and another EUV region appears in this area. Our objective here is to use multiple laser beams to initiate hydrodynamic confinement of the expanding laser plasma and to increase the total EUV radiation zone. The multiple laser beams compared to a single laser beam with the same total energy can yield higher EUV efficiency. Moreover, the optimal locations and angle of incidence of the laser beams can be obtained for various target geometries. Because many factors influence the final EUV conversion efficiency of the LPP devices by changing the target irradiation parameters, we initially identified the maximum efficient regime of a standard single-beam device to separate other contributions of plasma confinement in a multibeam assembly. In the case of positive input of the plasma confinement, the final CE of any multibeam configuration can be higher as in standard optimal case by the same total laser radiation energy, laser wavelength, pulse duration, and time distribution. The efficiency of a multibeam assembly should depend on the initial target form. We focused our simulations on two generally used target geometries: a droplet target and a plane target. A three-beam configuration of the LPP devices was selected for our

Downloaded 12 Dec 2006 to 140.221.12.207. Redistribution subject to AIP license or copyright, see http://jap.aip.org/jap/copyright.jsp

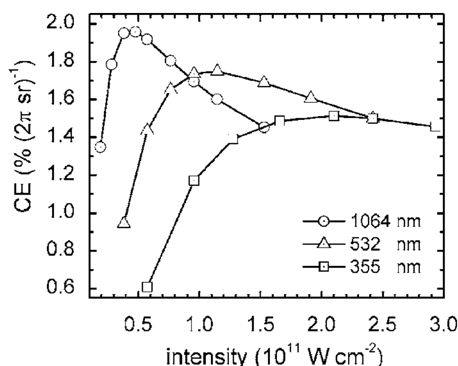

FIG. 3. Dependence of CE on laser irradiance for various laser wavelengths.

numerical simulation because of the small number of spatial orientation parameters (needed for optimization) and good capability for plasma confinement.

A. Droplet target case

Based on latest experiments and our preliminary calculations,[12,25,29] we used the following initial parameters for the single-beam droplet target device: a spherical tin target with a 100 μm diameter, a laser pulse with a total energy of up to 230 mJ, and duration of 10 ns. Three laser radiation wavelengths were analyzed for the optimization of EUV output: 355, 532, and 1064 nm. Both square and Gaussian time distributions of the laser pulse were simulated. Because the square pulse distribution in time produced higher CE, we only show results for the square pulse. The spatial distribution of laser radiation, however, was Gaussian for maximum EUV output. Therefore, the spatial distribution of the laser beam [see Eq. (11)] allowed to achieve laser power density is up to 3×10^{11} W/cm^2 with σ_s=50 μm used for initial parameters of the basic LPP device.

The efficiency of the single-beam LPP device model is shown in Fig. 3 as a function of radiation power density. The CE was calculated as the ratio of total EUV radiation output (13.5±2% nm band) into 2π sr solid angle to the energy of the initial laser pulse. As shown in Fig. 3, the maximum of the efficiency is obtained around $\sim(4.0-5.0)\times10^{10}$ W/cm^2 with a laser wavelength of 1064 nm. The optimum laser irradiance corresponds to total laser energy ~30–50 mJ irradiated in 10 ns as predicted by HEIGHTS simulations. The obtained optimum energy input, laser wavelength, and pulse duration were used for modeling the multibeam device. We distributed in equal parts the total laser energy among three different beams spatially located as schematically shown in Fig. 4. Laser beam spot sizes and shapes were equivalent to the single-beam laser spot size and shape. The radial angle φ among the different beams is taken to be 120°. This spatial configuration allows to limit the number of optimization parameters in this case to only the axial angle θ. Following our prediction, there should exist an axial angle $\theta>0°$ such that CE(θ)>CE(0°). The CE for the case of θ=0° corresponds to the standard single-beam device. The desired angle $\theta>0°$ will optimize the initiation of plasma confinement along the z axis and the formation of a larger EUV area.

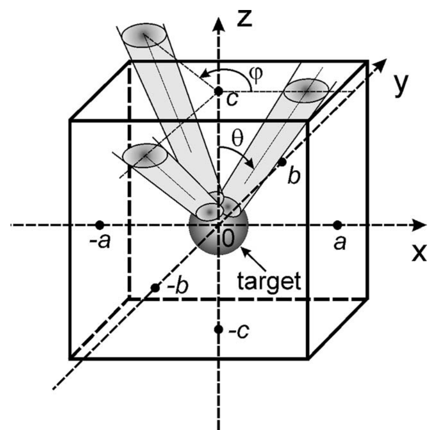

FIG. 4. Schematic illustration of multiple laser beams incident on target.

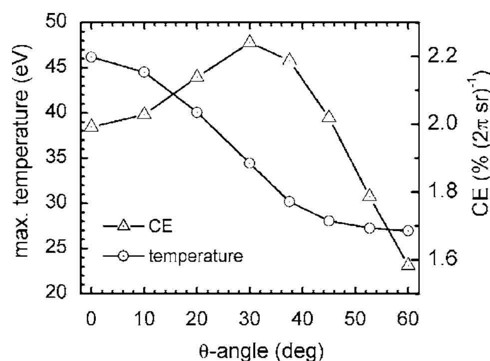

FIG. 5. Axial angle dependence of CE and maximum plasma temperature for the three-laser beam device.

Figure 5 shows the dependence of conversion efficiency on the axial angle for the three laser beams with a total laser energy of 45 mJ. The maximum temperature in the computational domain is presented just to show the redistribution of plasma parameters; i.e., areas with low densities are not overheated as in the single-beam case. As shown, the maximum CE was obtained at an axial angle of $\theta\approx30°$. The value of the CE was increased from 2.0%/2π sr for the single-beam case up to 2.24%/2π sr. To verify the optimum laser energy, the total energy dependence of the CE was simulated for θ=30° case. Figure 6 shows the CE results in comparison to the single laser beam efficiency. One can conclude that the three-beam configuration can be more effective than the single laser beam device having the same total en-

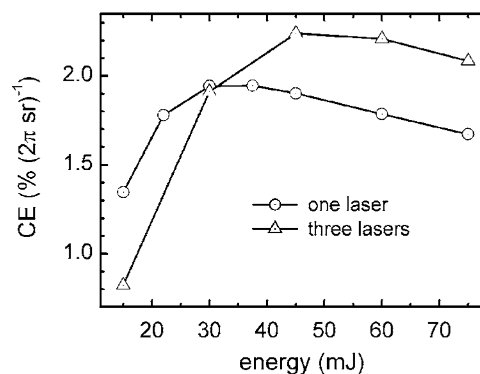

FIG. 6. Conversion efficiency of single and three-laser systems as a function of total laser energy.

Downloaded 12 Dec 2006 to 140.221.12.207. Redistribution subject to AIP license or copyright, see http://jap.aip.org/jap/copyright.jsp

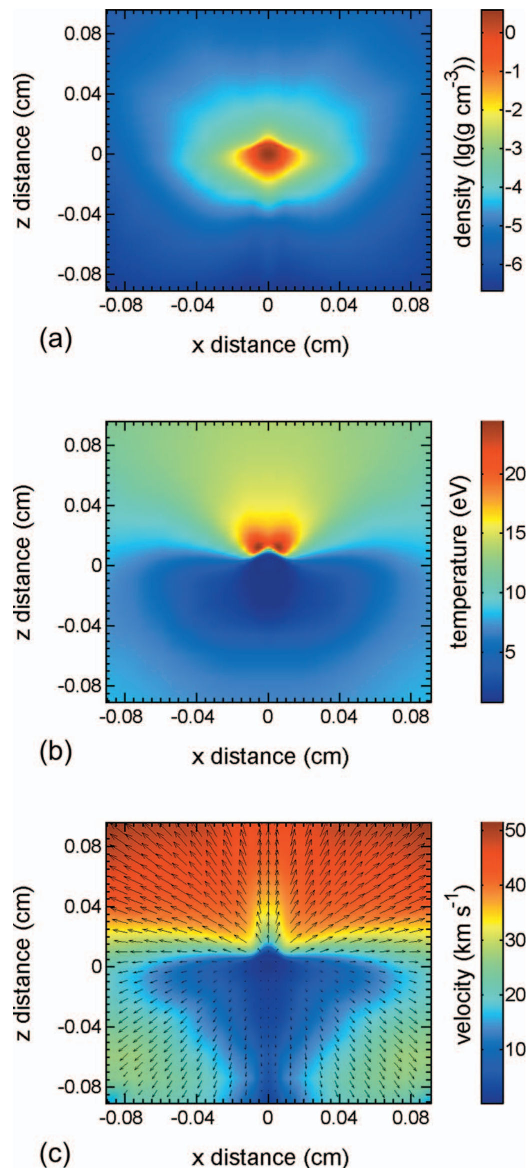

FIG. 7. (Color) Density (a), temperature (b), and velocity (c) of tin plasma in the *x*-*z* plane exposed to three laser beams of 45 mJ total energy and 10 ns pulse duration.

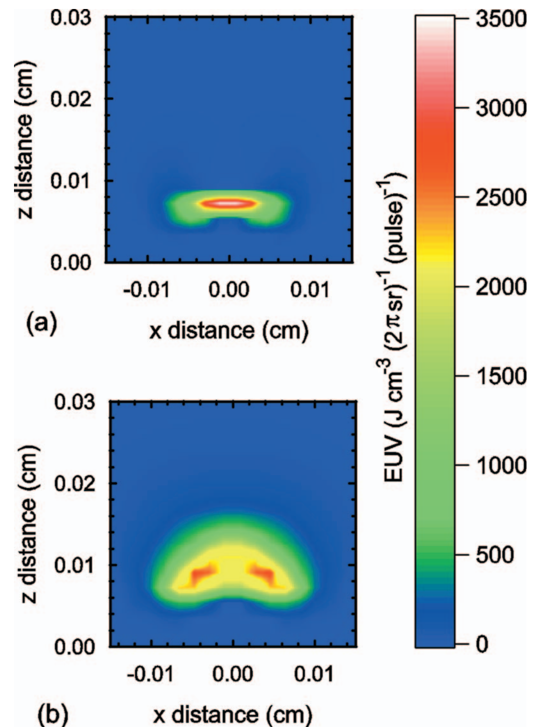

FIG. 8. (Color) *x*-*z* cross section of EUV radiation area for (a) one-laser and (b) three-laser beam systems incident on tin droplet target.

ergy. The higher CE advantage is mainly due to the three-dimensional spatial redistribution of the target plasma as shown in Fig. 7 for the *x*-*z* cross sections of the plasma density and temperature. The plasma modification of the resulting EUV area size and shape is shown in the lower graph of Fig. 8 for the three laser case. The EUV area is calculated from all EUV emitting volume cells into solid angle 2π sr. The droplet target center is located initially at the grid origin point.

B. Plane target case

The plane target is more conventional, easy to use, and is better examined in laser plasma experiments. We based our plane tin target simulations on the experimental work described in details in Ref. 30 Following this paper, we used radius $\sigma_s = 1.49 \times 10^{-2}$ cm for the single laser beam Gaussian distributed in space. As in the droplet target case, the time shape of the pulse was square and the optimum laser wavelength was 1064 nm. The duration of the laser pulse was taken to be equal to 7.5 ns. A total laser radiation energy of 0.3 J on the target surface produced an irradiance level of 5.73×10^{10} W/cm^2. As it was shown experimentally[30] and confirmed in our calculation, this is the optimum conditions for an EUV output at normal incidence of a laser beam on a target surface.

To confine the plasma expansion in the plane target case, we simulated the three-beam device schematically presented in Fig. 9. The single laser beam was split to three parallel beams, as shown in Fig. 9(a) in the *x*-*y* plane. The radial angle is taken to be 120°. This spatial configuration also limited the number of the optimization parameters to only one. The optimization parameter was expressed as the beam displacement ratio $\xi = R_1/R_0$. The case $\xi = 0$ corresponds to the basic single-beam LPP device, and following our prediction, there should exist a displacement ratio $\xi > 0$ such that $\mathrm{CE}(\xi) > \mathrm{CE}(0)$. Figure 10 shows the dependence of the final EUV conversion efficiency on the displacement ratio. The CE reaches a maximum value at the ξ ratio equal to ~ 0.9 and was increased from 2.17% up to 2.30%. The increase in the CE can be higher for different laser beam configurations, for example, by pyramidal arrangement of laser beams under the plane target surface. In these cases more than one optimization parameter exist, and these numerical simulations are being considered in our future work.

IV. CONCLUSIONS

We have developed an integrated model, HEIGHTS, to describe the hydrodynamics and optical processes that occur in LPP devices in full three-dimensional geometry. The

Downloaded 12 Dec 2006 to 140.221.12.207. Redistribution subject to AIP license or copyright, see http://jap.aip.org/jap/copyright.jsp

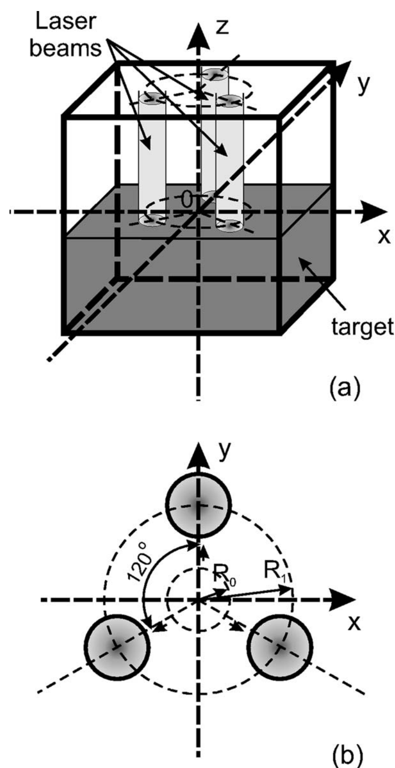

FIG. 9. Schematic illustration of three-laser beam numerical simulation setup with plane target: (a) spatial distribution of the laser beams; (b) *x-y* plane cross section. R_0 is the laser beam radius; R_1 is the displacement radius. Radial angle among laser displacement is equal to 120°.

model includes plasma heat conduction and hydrodynamic processes in a two-temperature approximation, as well as detailed photon radiation transport using three-dimensional Monte Carlo methods. We used HEIGHTS to simulate a three-beam laser system on a tin target as the light source for extreme ultraviolet lithography. The final EUV conversion efficiency is greatly influenced by the optimum correlation between plasma temperature and density. Comparison of the simulated plasma behavior with one and three laser beams indicates that the final CE of the LPP device can be increased by using plasma confinement spatial effects and by increasing the EUV radiation zone. Specifically, we were able to increase the CE of the tin droplet target LPP device from $2.0\%/2\pi$ sr for the one-beam case up to $2.24\%/2\pi$ sr, and the tin plane target LPP device from $2.17\%/2\pi$ up to

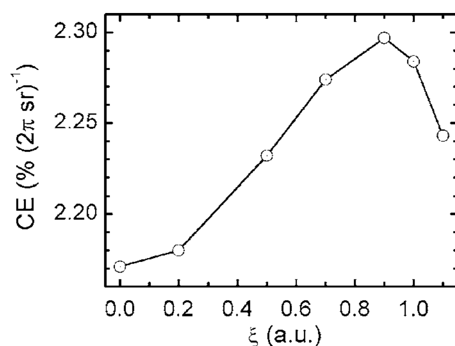

FIG. 10. Laser beam displacement ratio dependence of EUV conversion efficiency for three beams on tin plane target.

$2.3\%/2\pi$ sr. Further investigations of the effect of plasma confinement on the final CE of LPP devices should involve optimization of initial parameters: laser beam arrangement in space, laser power density distribution in time and in cross section of beam, laser pulse duration, target geometry, and target structure.

ACKNOWLEDGMENTS

The major part of this work was supported by Intel Corporation. Argonne National Laboratory is operated by the University of Chicago for the U.S. Department of Energy under Contract No. W-31-109-ENG-38.

[1] H. J. Levinson, *Principles of Lithography* (SPIE, Washington, 2001).
[2] D. Attwood, J. Phys. D **37** (2004).
[3] P. J. Silverman, Intel Technol. J. **6**, 55 (2002).
[4] V. Bakshi, in the Proceedings of the International SEMATECH EUV Source Workshop, Santa Clara, CA, 22 February 2004 (unpublished).
[5] U. Stamm, J. Phys. D **37**, 3213 (2004).
[6] J. Pankert, R. Apetz, K. Bergmann, A. List, M. Locken, C. Metzmacher, W. Neff, and S. Probst, Proc. SPIE **5751**, 260 (2005).
[7] D. W. Myers, I. V. Fomenkov, B. A. M. Hansson, B. C. Klene, and D. C. Brandt, Proc. SPIE **5751**, 248 (2005).
[8] T. Krücken, K. Bergmann, L. Juschkin, and R. Lebert, J. Phys. D **37**, 3213 (2004).
[9] M. Richardson, C.-S. Koay, K. Takenoshita, C. Keyser, S. George, S. Teerawattansook, M. Al-Rabban, and H. Scott, Proc. SPIE **5374**, 447 (2004).
[10] A. Hassanein, V. Sizyuk, V. Tolkach, V. Morozov, and B. J. Rice, J. Microlithogr., Microfabr., Microsyst. **3**, 130 (2004).
[11] A. Hassanein, V. Sizyuk, V. Tolkach, V. Morozov, T. Sizyuk, B. J. Rice, and V. Bakshi, Proc. SPIE **5374**, 413 (2004).
[12] V. Sizyuk, A. Hassanein, V. Morozov, V. Tolkach, T. Sizyuk, and B. Rice, Numer. Heat Transfer, Part A **49**, 215 (2006).
[13] G. V. Miloshevsky, V. A. Sizyuk, M. B. Partenskii, A. Hassanein, and P. C. Jordan, J. Comput. Phys. **212**, 25 (2006).
[14] S. I. Braginskii, in *Reviews of Plasma Physics*, edited by M. A. Leontovich (Consultants Bureau, New York, 1965), Vol. 1, p. 205.
[15] V. M. Kovenya, S. G. Cherny, and A. S. Lebedev, in *Computational Fluid Dynamics*, edited by G. S. Davis and C. Fletcher (North-Holland, Amsterdam, 1988).
[16] G. Tóth and D. Odstrčil, J. Comput. Phys. **128**, 82 (1996).
[17] R. J. Leveque, *Finite Volume Methods for Hyperbolic Problems* (Cambridge University Press, Cambridge, 2002).
[18] V. Morozov, V. Sizyuk, A. Hassanein, and V. Tolkach, Argonne National Laboratory Report No. ANL-ET-04/31, 2004 (unpublished).
[19] V. Morozov, V. Tolkach, and A. Hassanein, Argonne National Laboratory Report No. ANL-ET-04/24, 2004 (unpublished).
[20] M. von Allmen and A. Blatter, *Laser-Beam Interactions with Materials*, Springer Series in Material Science Vol. 2, 2nd ed. (Springer, Berlin, 1995).
[21] T. W. Johnston and J. M. Dawson, Phys. Fluids **16**, 722 (1973).
[22] L. Spitzer, *Physics of Fully Ionized Gases*, 2nd ed. (Interscience, New York, 1962).
[23] A. Hassanein, V. Sizyuk, V. Tolkach, V. Morozov, and B. J. Rice, Proc. SPIE **5037**, 714 (2003).
[24] T. Aota and T. Tomie, Phys. Rev. Lett. **94**, 015004 (2005).
[25] M. Richardson, C.-S. Koay, K. Takenoshita, C. Keyser, and M. Al-Rabban, J. Vac. Sci. Technol. B **22**, 785 (2004).
[26] I. W. Choi *et al.*, J. Opt. Soc. Am. B **17**, 1616 (2000).
[27] G. D. Kubiak, L. J. Bernardez II, K. D. Krenz, and W. C. Sweatt, Proc. SPIE **3676**, 669 (1999).
[28] S. Miyamoto, S. Amano, T. Inoue, A. Shimoura, K. Kaku, P.-E. Nica, H. Kinugasa, and T. Mochizuki, in Proceedings of the EUV Source Workshop, San Jose, California, 27 February 2005 (unpublished); http://www.sematech.org/meetings/archives.htm
[29] S. S. Harilal, B. O'Shay, M. S. Tillack, Y. Tao, R. Paguio, A. Nikroo, and C. A. Back, J. Phys. D **39**, 484 (2006).
[30] R. C. Spitzer, T. J. Orzechowski, D. W. Phillion, R. L. Kauffman, and C. Cerjan, J. Appl. Phys. **79**, 2251 (1996).

Downloaded 12 Dec 2006 to 140.221.12.207. Redistribution subject to AIP license or copyright, see http://jap.aip.org/jap/copyright.jsp